Volume 11
Number 24
28 June 2023
Pages 12407–13042

Journal of Materials Chemistry A

Materials for energy and sustainability

rsc.li/materials-a

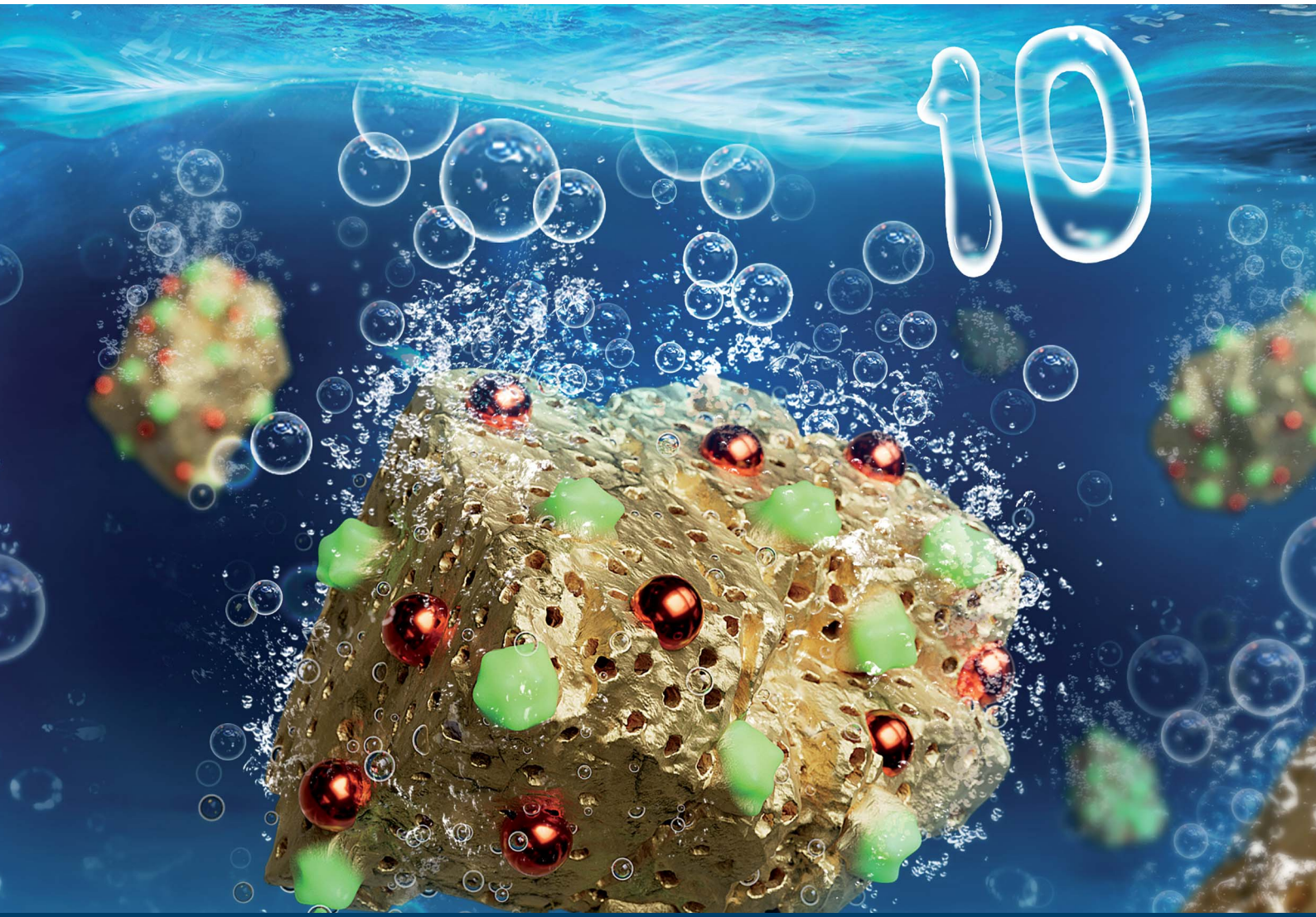

Themed issue: 10th Anniversary issue: Celebrating 10 years of Journal of Materials Chemistry A

ISSN 2050-7488

ROYAL SOCIETY OF CHEMISTRY

PAPER

Yang Song, Ping Wang, Jong-Beom Baek *et al.*
Controlled synthesis of highly active bifunctional electrocatalysts for overall water splitting using coal-based activated carbons

10 YEARS ANNIVERSARY

Journal of Materials Chemistry A

ROYAL SOCIETY OF CHEMISTRY

PAPER

View Article Online
View Journal | View Issue

Cite this: J. Mater. Chem. A, 2023, 11, 12726

Controlled synthesis of highly active bifunctional electrocatalysts for overall water splitting using coal-based activated carbons†

Xianglong Zhao,[a] Xinghua Yong,[a] Qizhe Ji,[a] Zhenghua Yang,[a] Yang Song, *[b] Yiqiang Sun, [c] Zhengyang Cai,[d] Jingcheng Xu,[e] Luyan Li,[a] Shuhua Shi,[a] Feiyong Chen,[b] Cuncheng Li, [c] Ping Wang *[d] and Jong-Beom Baek *[f]

Received 20th August 2022
Accepted 10th November 2022

DOI: 10.1039/d2ta06595a

rsc.li/materials-a

We report a facile approach for the synthesis of highly active bifunctional electrocatalysts for the oxygen evolution reaction (OER) and hydrogen evolution reaction (HER), by simply annealing mixtures of cheap coal-based activated carbons (CACs), ruthenium chloride and nickel chlorides in ammonia. The electrocatalysts consist of nitrogen doped CACs (NCACs), which are uniformly decorated with ruthenium (Ru) (with a low content of 0.3 wt%) and nickel nitride (Ni_3N) nanoparticles (Ni_3N/Ru/NCAC composites). The Ni_3N/Ru/NCAC composites have a large surface area (853 m^2 g^{-1}), which is proven to be attributable to the inherent large surface area of the CACs and the easy etching of CACs during an annealing process in ammonia. Electrochemical measurements reveal that OER electrocatalytic activities of the Ni_3N/Ru/NCAC composites remarkably outperform those of the state-of-the-art IrO_2 catalysts, and their HER activities were comparable to those of the benchmark Pt/C catalysts. Moreover, when the Ni_3N/Ru/NCAC composites are used as both anodes and cathodes of electrolyzers for overall water splitting (OWS), they delivered a lower voltage of 1.55 V at a current density of 10 mA cm^{-2} and better durability than Pt/C(−)//IrO_2(+) electrodes. These outstanding OER/HER bifunctional activities and OWS performances of the Ni_3N/Ru/NCAC composites are ascribed to the collaborative contributions of N, Ru, Ni_3N and their large surface areas.

10th anniversary statement

The *Journal of Materials Chemistry A* has been leading in the field of materials for future sustainable energy. The journal has played important roles in the realization of carbon neutrality. As an advisory board member, I sincerely congratulate the 10th anniversary of the *Journal of Materials Chemistry A* and continuously support its important contributions to the advancement of materials research studies to stand against climate change and realize net zero by 2050.

Introduction

Electrochemical water splitting is considered as a clean and sustainable method for producing high purity hydrogen.[1] However, the efficiency of overall water splitting (OWS) is hampered by its two half reactions, *i.e.*, the oxygen evolution reaction (OER) and the hydrogen evolution reaction (HER). This is because both of these reactions have sluggish reaction kinetics and a high reaction energy barrier.[2,3] Although noble metal based catalysts, such as ruthenium (Ru)/iridium (Ir)-based metal oxides (for the OER) and platinum (Pt)-based materials (for the HER), have demonstrated superior activity in OWS, their large-scale commercial applications have been hindered by their exorbitant cost and scarcity.[4,5] Hence, considerable efforts have been devoted to the fabrication of highly active OER/HER electrocatalysts with a minimum loading of noble metals or without them absolutely. In particular, electrocatalysts have been widely fabricated using carbon materials, such as carbon nanotubes (CNTs), graphene and carbon nanofibers. This is because: (1) carbon materials usually have the advantages of high electrical conductivity, large surface areas, and excellent chemical and environmental stability; and

[a]School of Science, Shandong Jianzhu University, Jinan, 250101, P. R. China
[b]Resources and Environment Innovation Institute, Shandong Jianzhu University, Jinan, 250101, P. R. China. E-mail: songyang20@sdjzu.edu.cn
[c]School of Chemistry and Chemical Engineering, University of Jinan, Jinan, 250022, P. R. China
[d]Energy Materials Research Center, Shanghai Institute of Ceramics, Chinese Academy of Sciences, Shanghai, 201899, P. R. China. E-mail: wangping@mail.sic.ac.cn
[e]School of Materials and Chemistry, University of Shanghai for Science and Technology, Shanghai, 200093, P. R. China
[f]School of Energy and Chemical Engineering, Center for Dimension-Controllable Organic Frameworks, Ulsan National Institute of Science and Technology (UNIST), Ulsan, 44919, Korea. E-mail: jbbaek@unist.ac.kr

† Electronic supplementary information (ESI) available. See DOI: https://doi.org/10.1039/d2ta06595a

(2) OER/HER activities of the carbon materials can be effectively boosted by incorporating heteroatoms (*e.g.*, nitrogen,[6] phosphorus,[7] and sulfur[8]), transition metals,[9] or transition metal oxides/nitrides/sulphides.[10–12]

Coal-based activated carbons (CACs) are a kind of commonly used activated carbons in daily life, and they are produced by using coals as feedstocks. Like other carbon materials, CACs also have high electrical conductivity and large surface areas.[13,14] More importantly, because of the massive reserves of coal on earth, the CACs have the remarkable advantages of low cost and high output (more than millions of tons are produced all over the world every year). Given these benefits, it would be of great significance for both scientific research and industrial applications to fabricate high-performance OER/HER bifunctional electrocatalysts using CACs.

Here, by simply annealing mixtures of CACs, ruthenium chloride and nickel chloride in the presence of ammonia, nitrogen doped CACs (NCACs) which were decorated with Ru and nickel nitride (Ni_3N) nanoparticles (denoted as Ni_3N/Ru/NCAC composites) were obtained. Electrochemical analyses revealed that the Ni_3N/Ru/NCAC composites had outstanding OER/HER bifunctional electrocatalytic activities and excellent OWS performances in alkaline media. These results were attributed to the synergic contributions from doped N, Ru, Ni_3N and their large surface areas. Specifically, the Ni_3N/Ru/NCAC composites delivered a lower overpotential of 288 mV at a current density of 10 mA cm^{-2} and a smaller Tafel slope of 60 mV dec^{-1} than the precious iridium oxide (IrO_2) catalysts (343 mV and 71 mV dec^{-1}) for the OER. They also exhibited an overpotential of 42 mV at 10 mA cm^{-2} and a Tafel slope of 59 mV dec^{-1} for the HER, both of which were close to those of the commercial Pt/C electrocatalysts (35 mV and 56 mV dec^{-1}). Furthermore, when Ni_3N/Ru/NCAC composites were employed as both anodes and cathodes of OWS electrolyzers, they demonstrated a lower cell voltage of 1.55 V at 10 mA cm^{-2} than Pt/C(−)//IrO_2(+) electrodes (1.59 V) as well as superior durability.

Results and discussion

Fig. 1a shows a schematic of the fabrication process of the Ni_3N/Ru/NCAC composites. First, mixed solutions of 0.07 M $RuCl_3$ and 0.15 M $NiCl_3$ were dropped on the CACs, followed by drying. Then, the samples were annealed in the presence of ammonia at 1000 °C. During this process, CACs were doped with nitrogen,[15] and ruthenium chloride was thermally reduced to Ru nanoparticles.[16] Meanwhile, nickel chloride was thermally reduced to Ni nanoparticles and further turned into Ni_3N nanoparticles.[17]

Fig. 1b and c show scanning electron microscope (SEM) images of the CACs and Ni_3N/Ru/NCAC composites,

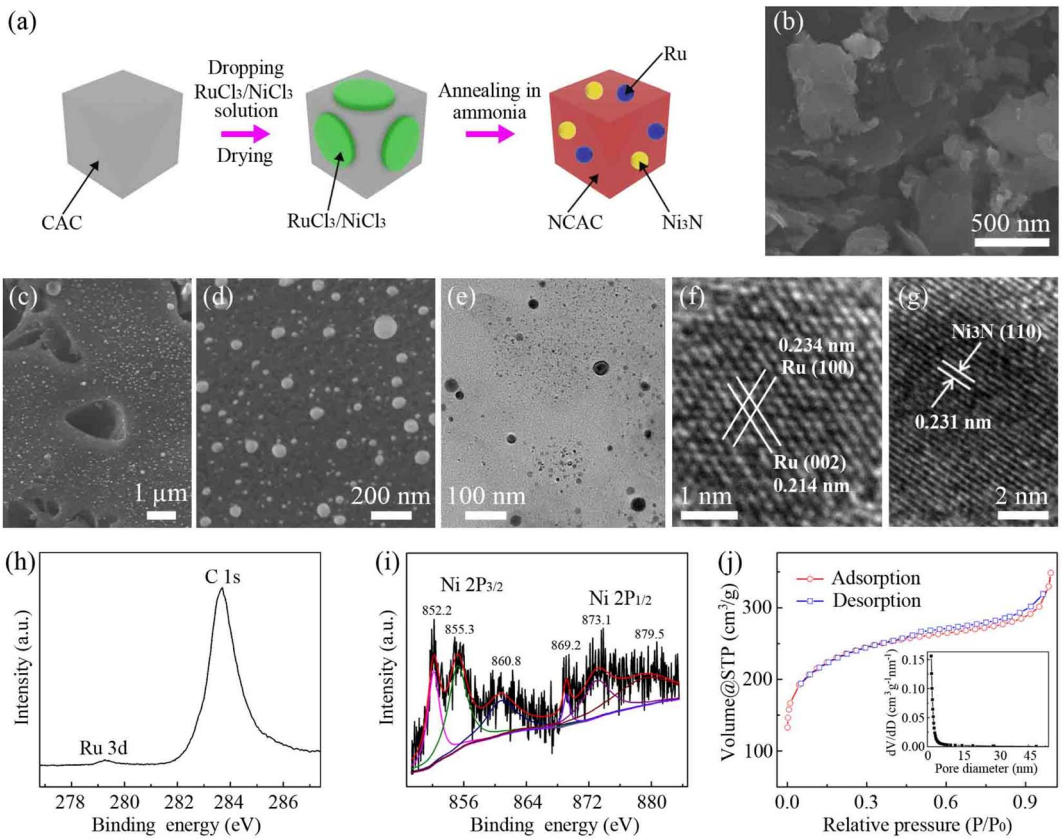

Fig. 1 (a) Schematics of fabrication of Ni_3N/Ru/NCAC composites. (b) High-magnification SEM image of CACs. (c–e) SEM, high-magnification SEM, and TEM images of Ni_3N/Ru/NCAC composites, respectively. HRTEM images: (f) Ru and (g) Ni_3N nanoparticles. High resolution XPS spectra: (h) Ru 3d and (i) Ni 2p. (j) Nitrogen adsorption–desorption isotherm of the Ni_3N/Ru/NCAC composites. Inset: Pore size distribution curve.

respectively. Fig. 1c shows that there are numerous Ru and Ni_3N nanoparticles anchored on the surfaces of the NCACs. The high-magnification SEM image (Fig. 1d) indicates that the sizes of these nanoparticles range from 15 to 110 nm. The transmission electron microscope (TEM) image (Fig. 1e) further confirms the decoration of Ru and Ni_3N nanoparticles on the NCACs. The high-resolution TEM (HRTEM) image of a Ru nanoparticle (Fig. 1f) shows that its inter-plane distances are 0.214 and 0.234 nm, which correspond to Ru (002) and Ru (100), respectively. The HRTEM image (Fig. 1g) of a Ni_3N nanoparticle clearly shows its (110) plane with an inter-plane distance of 0.231 nm, confirming that it mainly consists of Ni_3N. The elemental mappings (Fig. S1†) verify that the Ni_3N/Ru/NCAC composites are comprised of C, N, Ru and Ni elements. The X-ray photoelectron spectroscopy (XPS) spectrum (Fig. S2a†) suggests the presence of C and N but the absence of Ru and Ni in the Ni_3N/Ru/NCAC composites. This result confirms that nitrogen was doped in the CACs to form NCACs, and both Ru and Ni elements had low contents. A quantitative analysis was conducted using inductively coupled plasma mass spectrometry (ICP-MS), which showed that the contents of Ru and Ni elements were 0.3 and 2.7 wt%, respectively. The high resolution XPS spectra of the N 1s (Fig. S2b†) shows that the nitrogen can be deconvoluted into N^{3-} in Ni_3N (397.0 eV),[18] pyridinic N (398.6 eV)[19] and pyridinic N oxide (402 eV),[20] confirming again the nitrogen doping of CACs and the formation of Ni_3N. The high resolution XPS spectrum of Ru 3d (Fig. 1h) reveals a peak at 279.3 eV, indicative of the metallic Ru in the Ni_3N/Ru/NCAC composites.[21] The high resolution XPS spectra of Ni 2p reveal six peaks. The peaks at 852.2 and 869.2 eV are attributable to Ni^+ $2p_{3/2}$ and Ni^+ $2p_{1/2}$, respectively, and those at 860.8 and 879.5 eV are their corresponding satellite peaks. These results also confirm the existence of Ni_3N.[22] In addition, the peaks at 855.3 and 873.1 eV are assignable to nickel oxides, indicating the surface oxidization of Ni_3N.[22] But the X-ray diffraction (XRD) pattern result (Fig. S3†) verifies that the contents of these nickel oxides are almost negligible, and the predominant components of the nanoparticles on the NCACs are metallic Ru and Ni_3N. The Raman spectrum (Fig. S4†) reveals the higher intensity of the D band (1343 cm^{-1}) than the G band (1595 cm^{-1}), indicating the low crystallinity and high defect level of the Ni_3N/Ru/NCAC composites.[23] The nitrogen adsorption–desorption isotherms (Fig. 1j) of the Ni_3N/Ru/NCAC composites indicate that their Brunauer–Emmett–Teller (BET) surface areas are ~853 m^2 g^{-1}. As each factor of nitrogen doping,[24,25] incorporation with Ru and Ni_3N,[26–29] and large surface area[30,31] favored the electrocatalytic activity of carbon materials for the OER and HER, the combination of these factors in the Ni_3N/Ru/NCAC composites may endow the composites with high OER/HER bifunctional activities in OWS.

The OER electrocatalytic activity of the Ni_3N/Ru/NCAC composites was evaluated first. For comparison, those of the Ru/NCACs, NCACs, and CACs were also studied. Fig. 2a shows the linear sweep voltammetry (LSV) curves of these samples, which were recorded in oxygen saturated 0.1 M aq. KOH solutions. As expected, the Ni_3N/Ru/NCAC composites exhibited an overpotential of 288 mV at a current density of 10 mA cm^{-2} (η_{10}), which was lower than those of the Ru/NCACs (433 mV),

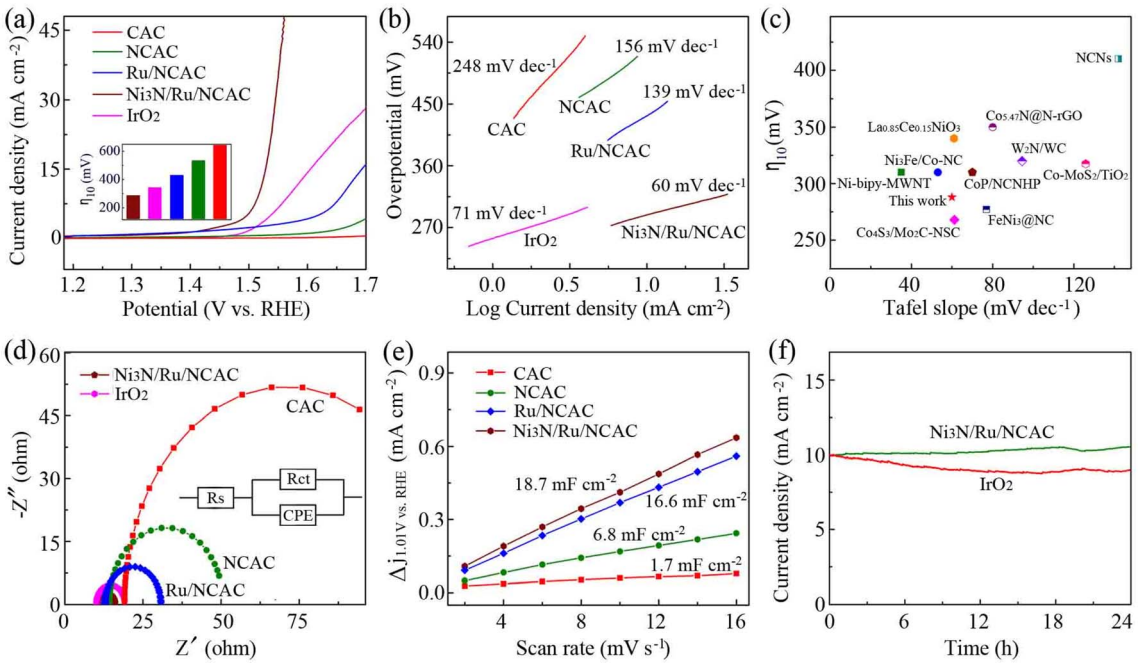

Fig. 2 (a) LSV curves of CACs, NCACs, Ru/NCACs, Ni_3N/Ru/NCAC composites and IrO_2 (scan rate: 5 mV s^{-1}). Inset: η_{10} for these samples. (b) Tafel plots of samples in (a). (c) Comparison of η_{10} and the corresponding Tafel slopes with those of many reported high-performance OER electrocatalysts. The corresponding references are listed in Table S1.† (d) Nyquist plots of samples in (a). (e) Calculations of C_{dl} for CACs, NCACs, Ru/NCACs and Ni_3N/Ru/NCAC composites. (f) Chronoamperometric curves of the Ni_3N/Ru/NCAC composites (at an overpotential of 288 mV) and IrO_2 (at an overpotential of 343 mV).

NCACs (535 mV) and CACs (>600 mV). This result confirms that the Ni_3N/Ru/NCAC composites have the best OER activity among these four samples, and the OER activity of these four samples is in the order of CACs < NCACs < Ru/NCACs < Ni_3N/Ru/NCAC composites. Also, this result indicates the negligible contributions of heteroatoms (such as S, Fig. S5†) in the CACs to the OER activity. Moreover, the excellent OER activity of the Ni_3N/Ru/NCAC composites reveals that all of the doped N, Ru and Ni_3N have played an important role. Specifically, N doping may modulate the electronic structures of the CACs, because nitrogen has stronger electronegativity than carbon.[32] The decorated Ru and Ni_3N nanoparticles on the NCACs may result in synergy between nanoparticles and NCACs. That is, there must be an efficient electron transfer from the conductive NCACs to Ru and Ni_3N nanoparticles.[27,33] In this case, the bond strength of oxygen-related intermediate species on surfaces of NCACs could be modulated, resulting in enhanced OER activity.[34] In addition, there appears to be a synergistic effect between the Ru and Ni_3N nanoparticles. This is evidenced by the remarkably enhanced OER activity of the Ni_3N/Ru/NCAC composites compared to both Ru/NCACs (the theoretical overpotentials of the Ni_3N/Ru/NCAC composites and Ru/NCACs were 1.849 and 2.069 eV, respectively, Fig. S6†) and Ni_3N/NCACs (η_{10}: 348 mV, Fig. S7†). This finding is consistent with the previous reports that different active components combined on carbon supports could have synergistic effects to boost OER activity.[35] More importantly, η_{10} of the Ni_3N/Ru/NCAC composites was lower than that (343 mV) of the state-of-the-art IrO_2 catalysts, confirming that the Ni_3N/Ru/NCAC composites had higher OER activity than IrO_2. In addition, the Tafel slope of the Ni_3N/Ru/NCAC composites was 60 mV dec^{-1}, which was also lower than those of IrO_2 (71 mV dec^{-1}), Ru/NCACs (139 mV dec^{-1}), NCACs (156 mV dec^{-1}), and CACs (248 mV dec^{-1}) (Fig. 2b). This result indicates that the Ni_3N/Ru/NCAC composites have the most favorable kinetics among these samples to drive the OER,[36] and their rate-determining step during the OER may be the second step, *i.e.*, $HO^* + OH^- \rightarrow H_2O + O^* + e$ (* represents the active site).[37] It is noteworthy that the Ni_3N/Ru/NCAC composites also exhibited better or comparable OER activity compared with previously reported OER electrocatalysts, including those fabricated using CNTs[38] and graphene[39] (Fig. 2c). Therefore, like CNTs and graphene, CACs can also be considered as qualified supports for the fabrication of highly active OER electrocatalysts.

Electrochemical impedance spectroscopy (EIS) measurement results (Fig. 2d) showed that the charge transfer resistance (R_{ct}) (5.6 Ω) of the Ni_3N/Ru/NCAC composites was lower than those of IrO_2 (9.2 Ω), Ru/NCACs (17.1 Ω), NCACs (36.6 Ω), and CACs (107.7 Ω), confirming that they obviously had the fastest electron transport.[40] Furthermore, electrochemical double-layer capacitances (C_{dl}) were recorded in the non-faradaic potential range using cyclic voltammetry (CV) (Fig. S8†) to evaluate the electrochemical surface area (ECSA).[41] The Ni_3N/Ru/NCAC composites exhibited a C_{dl} of 18.70 mF cm^{-2}, which is larger than those of the Ru/NCACs (16.6 mF cm^{-2}), NCACs (6.8 mF cm^{-2}), and CACs (1.7 mF cm^{-2}) (Fig. 2e). This result suggests that the Ni_3N/Ru/NCAC composites have significantly more active sites than the Ru/NCACs, NCACs and CACs,[42] confirming that doped N, Ru and Ni_3N nanoparticles provide more active sites for the adsorption of intermediates during the OER.[33,43,44] Moreover, the LSV curves of the CACs, NCACs, Ru/NCACs and Ni_3N/Ru/NCAC composites were normalized by ECSA, according to the C_{dl} values of the four samples. As shown in Fig. S9,† the OER activity of these four samples still demonstrated the same order of CACs < NCACs < Ru/NCACs < Ni_3N/Ru/NCAC composites. This indicates that, compared to the CACs, NCACs and Ru/NCACs, the superior OER activity of the Ni_3N/Ru/NCAC composites originated not only from the increased ECSA, but also from their optimized intrinsic activity.[45]

As durability is a critical parameter when evaluating the performances of OER electrocatalysts, the Ni_3N/Ru/NCAC composites were subjected to chronoamperometric measurements at a constant overpotential of 288 mV in 0.1 M aq. KOH solutions. As shown in Fig. 2f, the current densities of the Ni_3N/Ru/NCAC composites gradually increased, and were still higher than 10 mA cm^{-2} even after testing for 24 h. In contrast, the current densities of IrO_2 gradually decreased from 10 to 8.9 mA cm^{-2}. The higher OER durability of the Ni_3N/Ru/NCAC composites than IrO_2 catalysts suggests that the Ni_3N/Ru/NCAC composites are potential practical candidates for OER electrocatalysts. The characterization results (Fig. S10†) after the stability tests demonstrated that, during the OER process, the original pyridinic N in the NCACs was transformed into pyrrolic N,[46] and oxidization of Ru resulted in the formation of RuO_2 on surfaces of the Ru nanoparticles.[47] In addition, the oxidization of Ni_3N led to the formation of NiOOH on surfaces of the Ni_3N nanoparticles.[23] Hence, the real active sites of the Ni_3N/Ru/NCAC composites during the OER process could be the pyrrolic N, RuO_2 and NiOOH, and the synergistic effect of these active sites should be responsible for the high OER activity of the Ni_3N/Ru/NCAC composites.[48] Note that the contributions of N, Ru and Ni_3N to the OER activity of the Ni_3N/Ru/NCAC composites are in the order of N < Ru < Ni_3N (Fig. 2a). As a result, the contributions of pyrrolic N, RuO_2 and NiOOH active sites to the OER activity of the Ni_3N/Ru/NCAC composites should be in the order of pyrrolic N < RuO_2 < NiOOH. Moreover, the formation of these OER active species accounted for the current density increase during the OER stability test.[49] But the structures of the Ni_3N/Ru/NCAC composites during the OER were maintained, and their main compositions were clearly unchanged. The durability of the Ni_3N/Ru/NCAC composites was further confirmed by the small increase in η_{10} after 2000 CV cycles (Fig. S11†).

Next, the HER electrocatalytic activities of the Ni_3N/Ru/NCAC composites were evaluated by LSV curves in nitrogen saturated 1 M aq. KOH solutions. The η_{10} and η_{100} (overpotential at a current density of 10 and 100 mA cm^{-2}, respectively) of the Ni_3N/Ru/NCAC composites were 42 and 121 mV, respectively. The η_{10} for the Ru/NCACs, NCACs, and CACs were 88, 137 and >210 mV, respectively. Similar to the OER findings, the results indicate that the Ni_3N/Ru/NCAC composites had the best HER activity among these four samples, which benefitted from the significant contributions of doped N, Ru and Ni_3N (η_{10} of the Ni_3N/NCACs: 63 mV, Fig. S11†).[26,33] In addition, the η_{10} of the

Ni_3N/Ru/NCAC composites was very close to that (35 mV) of commercial Pt/C catalysts, indicating that Ni_3N/Ru/NCAC composites had comparable HER activity to Pt/C catalysts. The Tafel slope of the Ni_3N/Ru /NCAC composites was 59 mV dec^{-1}, which was marginally higher than that (56 mV dec^{-1}) of the Pt/C catalysts, but obviously lower than those of Ru/NCACs (74 mV dec^{-1}) and NCACs (140 mV dec^{-1}) (Fig. 3b). This result indicates that the HER process on the Ni_3N/Ru/NCAC composites followed the Volmer–Heyrovsky mechanism, where hydrogen desorption was considered to be the rate-determining step.[50,51] Moreover, the HER activity of the Ni_3N/Ru/NCAC composites outperformed or approached those of many recently reported HER electrocatalysts (Fig. 3c), including those consisting of CNT and graphene components.[52,53] This confirms again the superior HER activity of the Ni_3N/Ru/NCAC composites.

Consistent with the overpotential and Tafel slope results, EIS measurements (Fig. 3d) revealed that Ni_3N/Ru/NCAC composites possessed the smallest R_{ct} (0.8 Ω) compared to Ru/NCACs (1.8 Ω), NCACs (3.5 Ω), and CACs (21.9 Ω), indicating their efficient electron transfer during the HER. The turnover frequency (TOF) calculation results demonstrated that the TOF of the Ni_3N/Ru/NCAC composites was 0.36 H_2 per s, which was remarkably higher than those of the Ru/NCACs (0.07 H_2 per s) and NCACs (0.02 H_2 per s). Hence, Ni_3N/Ru/NCAC composites had the best intrinsic HER activity.[54] The chronoamperometric curves of the Ni_3N/Ru/NCAC composites showed that their current density dropped by less than 10% after testing for 24 h, suggesting their outstanding durability under HER conditions (Fig. S13†). The characterization results of the Ni_3N/Ru/NCAC composites after the HER stability test demonstrated that, except the formation of NiOOH on surfaces of Ni_3N nanoparticles,[55] there were almost no observed morphological and compositional changes of the composites (Fig. S14†).

In addition to 0.07 M $RuCl_3$ and 0.15 M $NiCl_3$, we also fabricated Ni_3N/Ru/NCAC composites using mixed solutions with both $RuCl_3$ and $NiCl_3$ having different concentrations. Electrochemical measurements (Fig. S15†) revealed that for the mixed solutions containing 0.02 M $RuCl_3$ and 0.05 M $NiCl_3$, the η_{10} of the Ni_3N/Ru/NCAC composites for the OER and HER was 360 and 68 mV, respectively. For those containing 0.2 M $RuCl_3$ and 0.4 M $NiCl_3$, the η_{10} of the composites for the OER and HER was 470 and 118 mV, respectively. Hence, these concentration variations of $RuCl_3$ and $NiCl_3$ resulted in lower OER/HER bifunctional activities of the Ni_3N/Ru/NCAC composites. ICP-MS measurements revealed that for 0.02 M $RuCl_3$ and 0.05 M $NiCl_3$, the contents of Ru and Ni in the Ni_3N/Ru/NCAC composites were 0.1 and 1.2 wt%, respectively. For 0.2 M $RuCl_3$ and 0.4 M $NiCl_3$, the contents of Ru and Ni were 1.3 and 10.5 wt%, respectively. Therefore, the combination of 0.07 M $RuCl_3$ and 0.15 M $NiCl_3$ was optimal for the synthesis of Ni_3N/Ru/NCAC composites with modest Ru and Ni (Ni_3N) contents

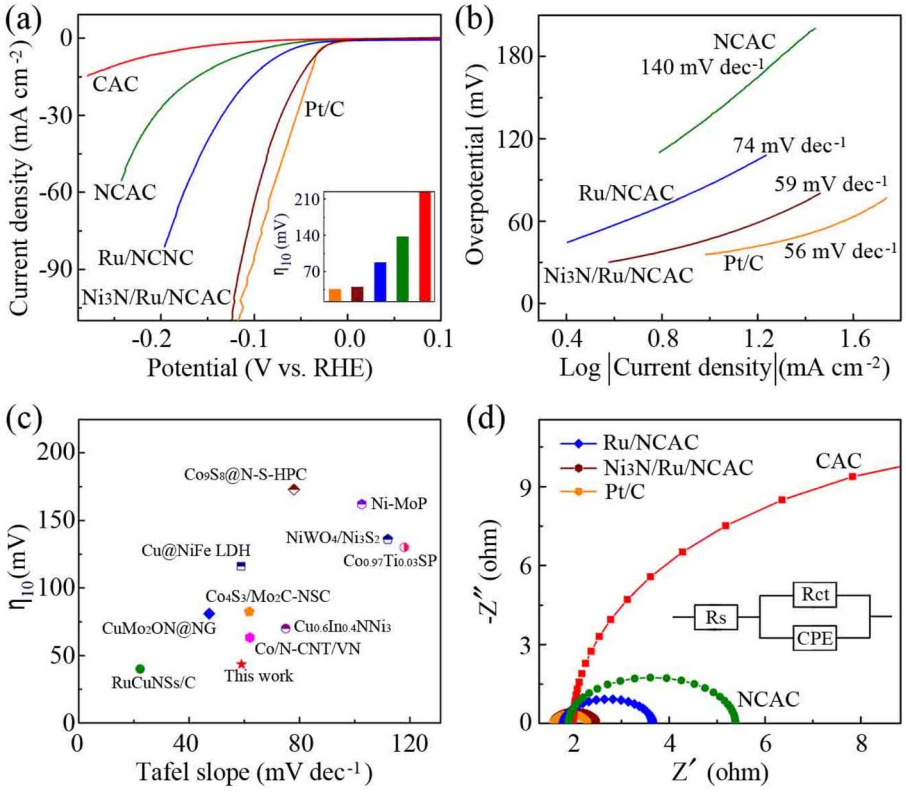

Fig. 3 (a) LSV curves of CACs, NCACs, Ru/NCACs, Ni_3N/Ru/NCAC composites and Pt/C catalysts (scan rate: 5 mV s^{-1}). Inset: η_{10} for these samples. (b) Tafel plots of samples in (a). (c) Comparison of η_{10} and the corresponding Tafel slopes with many reported high-performance HER electrocatalysts. The corresponding references are listed in Table S2.† (d) Nyquist plots of samples in (a).

to afford the enhanced OER/HER bifunctional activities. Similar findings have been reported on the Ir–Ni oxides.[56]

To better understand the outstanding nature of the CACs as a catalytic support, similar composites using wood based activated carbons (WACs) and coconut shell based activated carbons (SACs) were also prepared (Ni_3N/Ru/NWAC composites, Fig. S16;† Ni_3N/Ru/NSAC composites, Fig. S17†). For the OER, the measured η_{10}, Tafel slope and R_{ct} of the Ni_3N/Ru/NWAC composites were 560 mV, 154 mV dec^{-1} and 53 Ω, respectively, and those of the Ni_3N/Ru/NSAC composites were 400 mV, 134 mV dec^{-1} and 28.2 Ω, respectively (Fig. 4a and S18†). Therefore, in comparison with the Ni_3N/Ru/NCAC composites, the two catalytic composites displayed lower OER activity, inferior kinetics and slower electron transport during the OER. Similar to the OER, their HER activities were in the order of Ni_3N/Ru/NWAC (η_{10}: >350 mV; Tafel slope: 303 mV dec^{-1}; R_{ct}: 52.4 Ω) < Ni_3N/Ru/NSAC (110 mV, 107 mV dec^{-1} and 4.3 Ω) < Ni_3N/Ru/NCAC (Fig. 4b and S19†). Table S3† summarizes the contents of N, Ru and Ni elements and the BET surface areas of these three composites. In comparison with the differences in element contents, it was clearly observed that the differences in BET surface areas among these three composites were pretty remarkable. More importantly, the BET surface areas of these three composites follow the same order as their OER/HER bifunctional activities, *i.e.*, Ni_3N/Ru/NWAC (6 m^2 g^{-1}) < Ni_3N/Ru/NSAC (174 m^2 g^{-1}) < Ni_3N/Ru/NCAC (853 m^2 g^{-1}) (Fig. 4c). This result indicates that differences in surface area should be responsible for the discrepancy in the OER/HER bifunctional activities of these three composites. This finding is in line with the previous works that large surface areas benefited the OER/HER activities of carbon based electrocatalysts, because they provided more exposed active sites.[30,31]

According to a previous report, the surface area increase of the carbon materials during ammonia annealing resulted from the etching effects of nitrogen radicals.[57,58] Hence, we investigated the relationship between surface area of the CACs and their mass loss after ammonia annealing. As shown in Fig. 4d, e and Table S4,† after ammonia annealing, the BET surface areas of the CACs increased from 534 to 1246 m^2 g^{-1}, and their mass decreased from 300 to 120 mg. Therefore, annealing CACs in ammonia led to a BET surface area increase of 712 m^2 g^{-1} and a mass loss of 180 mg. In contrast, the BET surface area increase and the corresponding mass loss for WACs were only 1.6 m^2 g^{-1} and 35 mg, respectively, and those for SACs were 658 m^2 g^{-1} and 140 mg, respectively. These results indicate that in comparison with WACs and SACs, CACs had a higher response to the nitrogen radical attack. Raman spectra demonstrated that the CACs had a larger intensity ratio of the D band and G band (I_D/I_G: 1.10) than the WACs (0.55) and SACs (0.87) (Fig. 4f). This result reveals that the easy etching of the CACs during ammonia annealing could be ascribed to their inherently low crystallinity,[59] which originated from the well-known poor crystallinity of coals.[60] It is also noteworthy that the BET surface area (534 m^2 g^{-1}) of the CACs was also remarkably larger than those of WACs (7.2 m^2 g^{-1}) and SACs (75 m^2 g^{-1}) before ammonia annealing. This result may be attributable to the high porosity of CACs (the total pore volumes for CACs, WACs and SACs were 0.22, 0.04 and 0.017 cm^3 g^{-1}, respectively). We think the different porosities among CACs, WACs and SACs resulted from their different fabrication procedures and conditions. Overall, the intrinsic

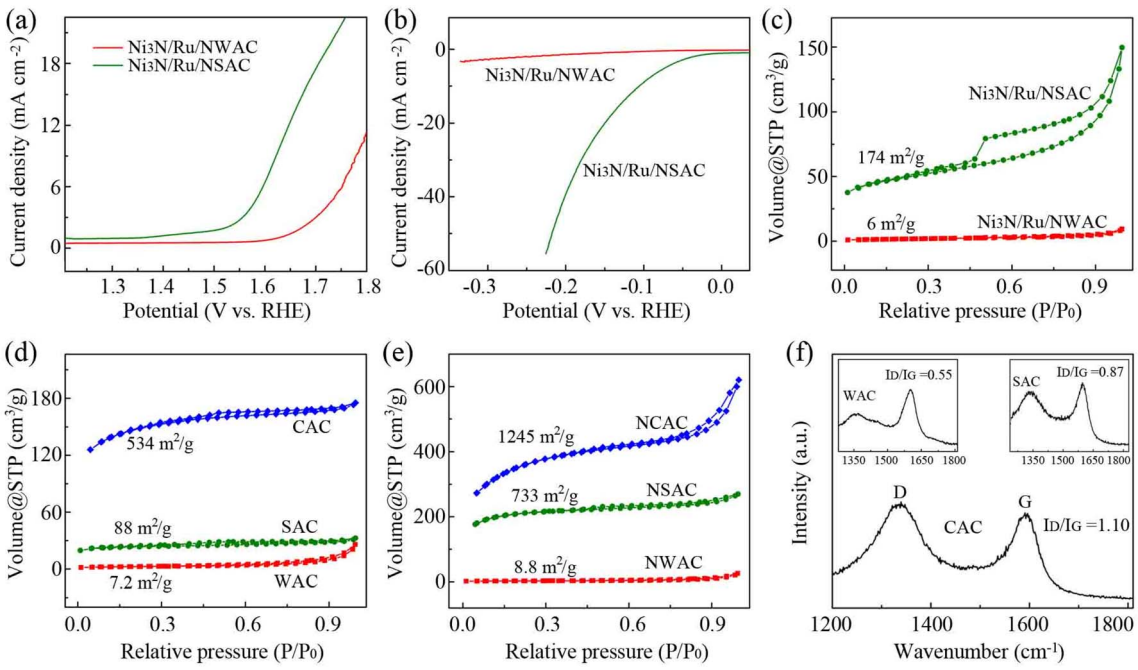

Fig. 4 (a, b) LSV curves of Ni_3N/Ru/NWAC and Ni_3N/Ru/NSAC composites for the OER and HER, respectively. Scan rate: 5 mV s^{-1}. (c–e) Nitrogen adsorption–desorption isotherms. (c) Ni_3N/Ru/NWAC and Ni_3N/Ru/NSAC composites. (d) WACs, SACs and CACs. (e) NWACs, NSACs and NCACs. (f) Raman spectra of WACs, SACs and CACs.

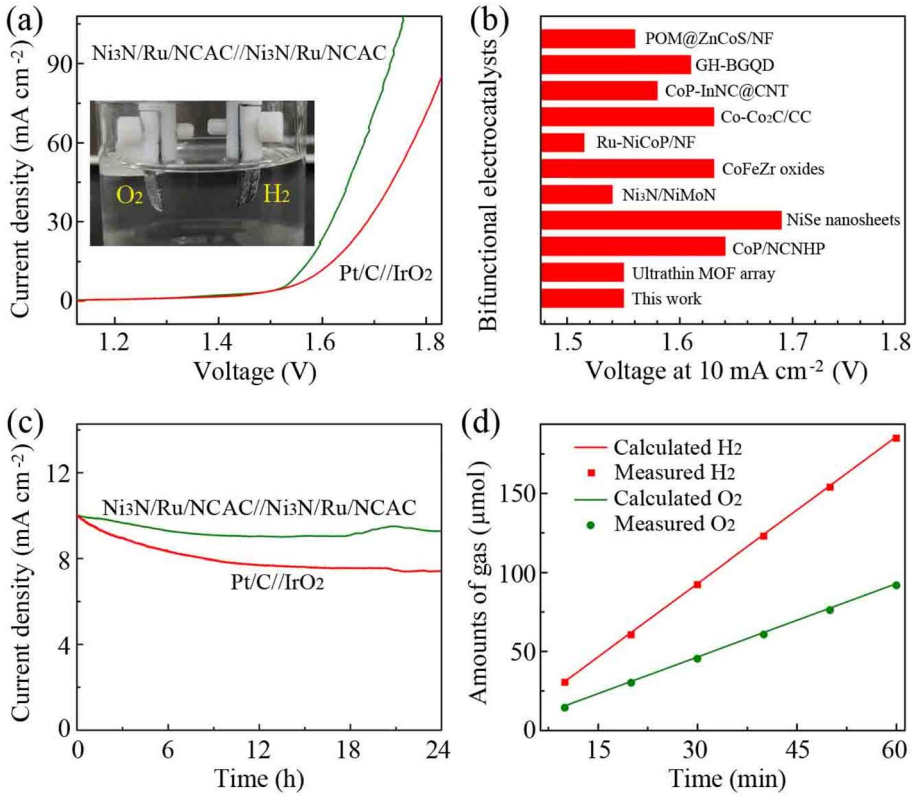

Fig. 5 OWS performances of Ni_3N/Ru/NCAC composites in 1 M KOH. (a) LSV curves (scan rate: 5 mV s^{-1}). Inset: Photograph showing the evolved H_2 and O_2 on the electrodes. (b) Comparison of the voltages at a current density of 10 mA cm^{-2} with those of recently reported bifunctional electrocatalysts. The corresponding references are given in Table S5.† (c) Chronoamperometric curves of Ni_3N/Ru/NCAC//Ni_3N/Ru/NCAC (at a constant voltage of 1.55 V) and Pt/C//IrO_2 electrolyzers (at a constant voltage of 1.59 V). (d) Amounts of the evolved H_2 and O_2 as a function of time.

large surface areas of the CACs together with their remarkably increased surface areas after ammonia annealing are responsible for the enhanced OER/HER activities of the Ni_3N/Ru/NCAC composites compared to the Ni_3N/Ru/NWAC and Ni_3N/Ru/NSAC composites.

Moreover, the Ni_3N/Ru/NCAC composites demonstrated better OER/HER bifunctional electrocatalytic activities than the Ni_3N/Ru/NCNT composites (for the OER, η_{10}: 322 mV, Tafel slope: 115 mV dec^{-1}, R_{ct}: 9.9 Ω; for the HER, η_{10}: 67 mV, Tafel slope: 72 mV dec^{-1}, R_{ct}: 1.2 Ω) (Fig. S21 and S22†), which were fabricated using commercial CNTs and a similar ammonia annealing process. The large surface areas of the Ni_3N/Ru/NCAC composites could also play a critical role (BET surface area of the Ni_3N/Ru/NCNT composites: 138 m^2 g^{-1}). More importantly, in view of the overwhelming superiority of the CACs to CNTs in terms of cost and yield, this result indicates that CACs are more desirable than CNTs for the fabrication of highly active OER/HER bifunctional electrocatalysts.

Because the Ni_3N/Ru/NCAC composites had excellent OER/HER bifunctional activities, a two-electrode electrolyzer was fabricated for OWS, with Ni_3N/Ru/NCAC composites as both anode and cathode. Electrochemical measurements revealed that the electrolyzer exhibited a current density of 10 mA cm^{-2} at a cell voltage of 1.55 V. This voltage was lower than that (1.59 V) generated on the electrolyzer using Pt/C(−)//IrO_2(+) (Fig. 5a), and it was also lower than or close to those delivered on electrolyzers assembled using previously reported OER/HER bifunctional catalysts (Fig. 5b). This result indicates that the Ni_3N/Ru/NCAC composites are superb bifunctional electrocatalysts for OWS. The chronoamperometry tests revealed that the current density of the Ni_3N/Ru/NCAC//Ni_3N/Ru/NCAC electrolyzer dropped by only 7% after 24 h (Fig. 5c), while that of the Pt/C//IrO_2 electrolyzer dropped by more than 25%. Therefore, the Ni_3N/Ru/NCAC//Ni_3N/Ru/NCAC electrolyzer had superior durability for OWS. Furthermore, faradaic efficiency of the Ni_3N/Ru/NCAC composite electrodes was studied by measuring evolved amounts of H_2 and O_2 using gas chromatography (GC). As illustrated in Fig. 5d, the experimentally measured ratio of evolved H_2 and O_2 is about 2 : 1, which agrees well with the theoretically calculated result. Hence, the faradaic efficiency of the Ni_3N/Ru/NCAC composites for OWS was nearly 100%.

Conclusions

In summary, electrocatalysts consisting of NCACs decorated with Ru (at a low content of 0.3 wt%) and Ni_3N nanoparticles were synthesized, by annealing mixtures of CACs, nickel chlorides and ruthenium chloride in the presence of ammonia. The resulting Ni_3N/Ru/NCAC composites had large surface areas, which resulted from the intrinsic large surface areas of the CACs

and the easy etching of CACs during ammonia annealing. The electrochemical measurement results demonstrated that the Ni_3N/Ru/NCAC composites possessed a lower overpotential of 288 mV at a current density of 10 mA cm^{-2} and better durability than the state-of-the-art IrO_2 catalysts for the OER. They also had an overpotential of 42 mV at 10 mA cm^{-2} for the HER, which was close to that of the benchmark Pt/C catalysts. Moreover, when they were utilized as bifunctional electrocatalysts for OWS, they exhibited a low cell voltage of 1.55 V at 10 mA cm^{-2}, excellent durability and a nearly 100% faradaic efficiency. The superior bifunctional electrocatalytic performances of the Ni_3N/Ru/NCAC composites were proven to derive from the collaborative contributions of N, Ru, Ni_3N and their large surface areas. This is, to the best of our knowledge, the first report on the synthesis of highly active OER/HER bifunctional electrocatalysts using cheap CACs, and this work may open up opportunities for CACs to be applied in OWS fields. Furthermore, given the virtues of low cost and extremely high availability of CACs as well as the easy fabrication of Ni_3N/Ru/NCAC composites, this work may also provide an attractive strategy for the design and synthesis of low-cost and high-performance OER/HER bifunctional electrocatalysts. Moreover, in comparison with the current coal gasification approach,[61] our work may offer an absolutely new methodology for employing coal in the production of hydrogen.

Author contributions

X. Z., S. S. and F. C. designed the experiments. X. Y. and Q. J. carried out the experiments for the fabrication of different composites. Z. Y. and Z. C. performed the electrochemical measurements. J. X. conducted the theoretical calculations. Y. S., Y. S. and P. W. analyzed the data. L. L., C. L. and J. B. wrote the manuscript. All the authors contributed to the discussion of the results and revised the manuscript.

Conflicts of interest

There are no conflicts to declare.

Acknowledgements

This work was financially supported by the National Key Research and Development Program of China (2022YFE0105800), Nanxun Collaborative Innovation Center Key Research Project (SYS01001), and Special Research Funds of Shandong Jianzhu University (No. X20077Z0101 and X20087Z0101). Also, the authors are thankful to the financial support from the Creative Research Initiative (CRI, 2014R1A3A2069102) and the Science Research Center (SRC, 2016R1A5A1009405) programs through the National Research Foundation (NRF) of Korea.

Notes and references

1 J. A. Turner, *Science*, 2004, **305**, 972.
2 Y. Yang, H. Yao, Z. Yu, S. M. Islam, H. He, M. Yuan, Y. Yue, K. Xu, W. Hao, G. Sun, H. Li, S. Ma, P. Zapol and M. G. Kanatzidis, *J. Am. Chem. Soc.*, 2019, **141**, 10417.
3 H. Zhou, F. Yu, J. Sun, R. He, S. Chen, C. Chu and Z. Ren, *Proc. Natl. Acad. Sci. U. S. A.*, 2017, **114**, 5607.
4 H. Jiang, Y. Liu, W. Li and J. Li, *Small*, 2018, **14**, 1703739.
5 H. Wang, S. Min, Q. Wang, D. Li, G. Casillas, C. Ma, Y. Li, Z. Liu, L. Li, J. Yuan, M. Antonietti and T. Wu, *ACS Nano*, 2017, **11**, 4358.
6 X. Zou, X. Huang, A. Goswami, R. Silva, B. R. Sathe, E. Mikmekov and T. Asefa, *Angew. Chem., Int. Ed.*, 2014, **53**, 4372.
7 Y. Hou, M. Qiu, T. Zhang, J. Ma, S. Liu, X. Zhuang, C. Yuan and X. Feng, *Adv. Mater.*, 2017, **29**, 1604480.
8 Y. Ito, W. Cong, T. Fujita, Z. Tang and M. Chen, *Angew. Chem., Int. Ed.*, 2015, **54**, 2131.
9 X. Cui, P. Ren, D. Deng, J. Deng and X. Bao, *Energy Environ. Sci.*, 2016, **9**, 123.
10 Y. Liang, Y. Li, H. Wang, J. Zhou, J. Wang, T. Regier and H. Dai, *Nat. Mater.*, 2011, **10**, 780.
11 W. Yuan, S. Wang, Y. Ma, Y. Qiu, Y. An and L. Cheng, *ACS Energy Lett.*, 2020, **5**, 692.
12 K. Jayaramulu, J. Masa, O. Tomanec, D. Peeters, V. Ranc, A. Schneemann, R. Zboril, W. Schuhmann and R. A. Fischer, *Adv. Funct. Mater.*, 2017, **27**, 1700451.
13 G. Gryglewicz, J. Machnikowski, E. Lorenc-Grabowska, G. Lota and E. Frackowiak, *Electrochim. Acta*, 2005, **50**, 1197.
14 D. Dong, Y. Zhang, Y. Xiao, T. Wang, J. Wang, C. E. Romero and W. Pan, *J. Colloid Interface Sci.*, 2020, **580**, 77.
15 N. A. Travlou, C. Ushay, M. Seredych, E. Rodríguez-Castellón and T. J. Bandosz, *ACS Sens.*, 2016, **1**, 591.
16 P. Zhang, F. Zhu, X. Tan, W. Li, S. Xu, P. Zhang, C. Wei and S. Miao, *Appl. Clay Sci.*, 2018, **166**, 207.
17 Y. Jia, H. Pan, H. Meng, H. Liu, Z. Wang, X. Li, L. Zhu, P. Chai and C. Gong, *RSC Adv.*, 2015, **5**, 14061.
18 Y. Yu, W. Gao, Z. Shen, Q. Zheng, H. Wu, X. Wang, W. Song and K. Ding, *J. Mater. Chem. A*, 2015, **3**, 16633.
19 Z. Wu, S. Yang, Y. Sun, K. Parvez, X. Feng and K. Müllen, *J. Am. Chem. Soc.*, 2012, **134**, 9082.
20 B. Li, F. Dai, Q. Xiao, L. Yang, J. Shen, C. Zhang and M. Cai, *Energy Environ. Sci.*, 2016, **9**, 102.
21 V. Mazzieri, F. Coloma-Pascual, A. Arcoya, P. C. L'Argentière and N. S. Fígoli, *Appl. Surf. Sci.*, 2003, **210**, 222.
22 Y. Wang, L. Chen, X. Yu, Y. Wang and G. Zheng, *Adv. Energy Mater.*, 2017, **7**, 1601390.
23 M. Chen, J. Qi, D. Guo, H. Lei, W. Zhang and R. Cao, *Chem. Commun.*, 2017, **53**, 9566.
24 X. Zhao, F. Li, R. Wang, J. Seo, H. Choi, S. Jung, J. Mahmood, I. Jeon and J. Baek, *Adv. Funct. Mater.*, 2017, **27**, 1605717.
25 Y. Yang, Z. Lun, G. Xia, F. Zheng, M. He and Q. Chen, *Energy Environ. Sci.*, 2015, **8**, 3563.
26 D. H. Kweon, M. S. Okyay, S. Kim, J. Jeon, H. Noh, N. Park, J. Mahmood and J. Baek, *Nat. Commun.*, 2020, **11**, 1278.
27 T. Gao, X. Li, X. Chen, C. Zhou, Q. Yue, H. Yuan and D. Xiao, *Chem. Eng. J.*, 2021, **424**, 130416.
28 T. Liu, M. Li, C. Jiao, M. Hassan, X. Bo, M. Zhou and H. Wang, *J. Mater. Chem. A*, 2017, **5**, 9377.

29 W. Ni, A. Krammer, C. Hsu, H. M. Chen, A. Schüler and X. Hu, *Angew. Chem., Int. Ed.*, 2019, **58**, 7445.
30 H. Jiang, J. Gu, X. Zheng, M. Liu, X. Qiu, L. Wang, W. Li, Z. Chen, X. Ji and J. Li, *Energy Environ. Sci.*, 2019, **12**, 322.
31 J. Wang, Z. Wei, S. Mao, H. Li and Y. Wang, *Energy Environ. Sci.*, 2018, **11**, 800.
32 W. J. Lee, U. N. Maiti, J. M. Lee, J. Lim, T. H. Han and S. O. Kim, *Chem. Commun.*, 2014, **50**, 6818.
33 C. Huang, B. Zhang, Y. Wu, Q. Ruan, L. Liu, J. Su, Y. Tang, R. Liu and P. K. Chu, *Appl. Catal., B*, 2021, **297**, 120461.
34 T. Lu, C. Chen, Y. Lu, C. Dong and R. Liu, *J. Phys. Chem. C*, 2016, **120**, 28093.
35 M. Yang, T. Feng, Y. Chen, J. Liu, X. Zhao and B. Yang, *Appl. Catal., B*, 2020, **267**, 118657.
36 Q. Shi, Q. Liu, Y. Ma, Z. Fang, Z. Liang, G. Shao, B. Tang, W. Yang, L. Qin and X. Fang, *Adv. Energy Mater.*, 2020, **10**, 1903854.
37 N. Suen, S. Hung, Q. Quan, N. Zhang, Y. Xu and H. Chen, *Chem. Soc. Rev.*, 2017, **46**, 337.
38 M. Tavakkoli, M. Nosek, J. Sainio, F. Davodi, T. Kallio, P. M Joensuu and K. Laasonen, *ACS Catal.*, 2017, **7**, 8033.
39 X. Shu, S. Chen, S. Chen, W. Pan and J. Zhang, *Carbon*, 2020, **157**, 234.
40 L. Yu, H. Zhou, J. Sun, F. Qin, F. Yu, J. Bao, Y. Yu, S. Chen and Z. Ren, *Energy Environ. Sci.*, 2017, **10**, 1820.
41 Z. Cai, X. Bu, P. Wang, W. Su, R. Wei, J. C. Ho, J. Yang and X. Wang, *J. Mater. Chem. A*, 2019, **7**, 21722.
42 H. Wu, X. Lu, G. Zheng and G. W. Ho, *Adv. Energy Mater.*, 2018, **8**, 1702704.
43 X. Cui, P. Ren, D. Deng, J. Deng and X. Bao, *Energy Environ. Sci.*, 2016, **9**, 123.
44 G. Li, K. Zheng, W. Li, Y. He and C. Xu, *ACS Appl. Mater. Interfaces*, 2020, **12**, 51437.
45 F. Yuan, J. Wei, G. Qin and Y. Ni, *J. Alloys Compd.*, 2020, **830**, 154658.
46 Y. Ha, B. Fei, X. Yan, H. Xu, Z. Chen, L. Shi, M. Fu, W. Xu and R. Wu, *Adv. Energy Mater.*, 2020, **10**, 2002592.
47 J. Li, M. Huang, X. Chen, L. Kong, Y. Zhou, M. Wang, J. Li, Z. Wu and X. Xu, *Chem. Commun.*, 2020, **56**, 6802.
48 S. Li, B. Chen, Y. Wang, M. Ye, P. A. Aken, C. Cheng and A. Thomas, *Nat. Mater.*, 2021, **20**, 1240.
49 G. Chen, T. Ma, Z. Liu, N. Li, Y. Su, K. Davey and S. Qiao, *Adv. Funct. Mater.*, 2016, **26**, 3314.
50 Y. Zheng, Y. Jiao, M. Jaroniec and S. Z. Qiao, *Angew. Chem., Int. Ed.*, 2015, **54**, 52.
51 Y. Sun, K. Mao, Q. Shen, L. Zhao, C. Shi, X. Li, Y. Gao, C. Li, K. Xu and Y. Xie, *Adv. Funct. Mater.*, 2022, **32**, 2109792.
52 C. Huang, D. Wu, P. Qin, K. Ding, C. Pi, Q. Ruan, H. Song, B. Gao, H. Chen and P. K. Chu, *Nano Energy*, 2020, **73**, 104788.
53 J. Balamurugan, T. T. Nguyen, N. H. Kim, D. H. Kim and J. H. Lee, *Nano Energy*, 2021, **85**, 105987.
54 Y. Sun, X. Li, T. Zhang, K. Xu, Y. Yang, G. Chen, C. Li and Y. Xie, *Angew. Chem., Int. Ed.*, 2021, **60**, 21575.
55 X. Shang, K. Yan, Y. Rao, B. Dong, J. Chi, Y. Liu, X. Li, Y. Chai and C. Liu, *Nanoscale*, 2017, **9**, 12353.
56 T. Reier, Z. Pawolek, S. Cherevko, M. Bruns, T. Jones, D. Teschner, S. Selve, A. Bergmann, H. N. Nong, R. Schlögl, K. J. J. Mayrhofer and P. Strasser, *J. Am. Chem. Soc.*, 2015, **137**, 13031.
57 H. Liang, Z. Wu, L. Chen, C. Li and S. Yu, *Nano Energy*, 2015, **11**, 366.
58 W. Shen and W. Fan, *J. Mater. Chem. A*, 2013, **1**, 999.
59 N. Yoshizawa, K. Maruyama, Y. Yamada and M. Zielinska-Blajet, *Fuel*, 2000, **79**, 1461.
60 J. Jiang, W. Yang, Y. Cheng, Z. Liu, Q. Zhang and K. Zhao, *Fuel*, 2019, **239**, 559.
61 A. Midilli, H. Kucuk, M. E. Topal, U. Akbulut and I. Dincer, *Int. J. Hydrogen Energy*, 2021, **46**, 25385.

